RF MEMs Variable Capacitors for Tunable Filters

Charles L. Goldsmith, Andrew Malczewski, Zhimin J. Yao, Shea Chen, John Ehmke, David H. Hinzel

Raytheon Systems Corporation, 13510 N. Central Expressway, MS 35 Dallas, Texas 75243

Received 27 July 1998; revised 30 December 1998

ABSTRACT: An RF MEMs (microelectromechanical system) variable capacitor has been demonstrated with a 22:1 tuning range, tuning from 1.5 to 33.2 pF of capacitance. This capacitor was constructed using bistable MEMs membrane capacitors with individual tuning ranges of 70:1 to 100:1, control voltages in the 30–55 V range, switching speeds less than 10 μS, and operating frequencies as high as 40 GHz. These devices may eventually provide a viable alternative to electronic varactors with improved tuning range and lower loss. © 1999 John Wiley & Sons, Inc. Int J RF and Microwave CAE 9: 362–374, 1999.

Keywords: MEMs; microelectromechanical system; tunable capacitors varactors; membrane capacitor; tunable filter

I. INTRODUCTION

Variable capacitors are important control elements in many high frequency radio receivers and transmitters. The most common application of tunable capacitors (varactors) in these radios is as tunable filters and oscillators. Tunable circuits such as these commonly require a wide tuning range and high quality factor (high Q) from the control element. The advent of MEMs technology for RF applications enables new and exciting possibilities for creating and controlling capacitance with wide tuning range and high Q. This is due to the unique capabilities enabled by micromechanical tuning and the low loss materials used in the construction of RF MEMs devices. Several analog MEMs tuning methods have been demonstrated to date [1–4]. Unfortunately, these devices exhibited either a limited tuning range of less than 2:1 [1–3] or a very slow tuning scheme [4]. Modern receiver architectures require large tuning ranges and quick switching times. This paper presents a micromechanical capacitive tuning technique yielding bistable, digital capacitance selection with tuning ranges greater than 20:1 and tuning speeds on the order of microseconds.

II. MEMs CAPACITOR CONSTRUCTION

The cross section of a metal membrane variable capacitor is shown in Figure 1a. The RF MEMs capacitor consists of a lower electrode fabricated on the surface of the IC and a thin aluminum membrane suspended over the electrode. The membrane is connected directly to grounds on either side of the electrode while a thin dielectric layer covers the lower electrode. The air gap between the two conductors determines the MEMs capacitor off-capacitance. With no applied actuation potential, the residual tensile stress of the membrane keeps it suspended above the RF path. Application of a DC electrostatic field to the lower electrode causes the formation of positive and negative charges on the electrode and membrane conductor surfaces. These charges exhibit an attractive force which, when strong enough, causes the suspended metal membrane to snap down onto the lower electrode and dielec-

Correspondence to: C. Goldsmith

CCC 1096-4290/99/040362-13

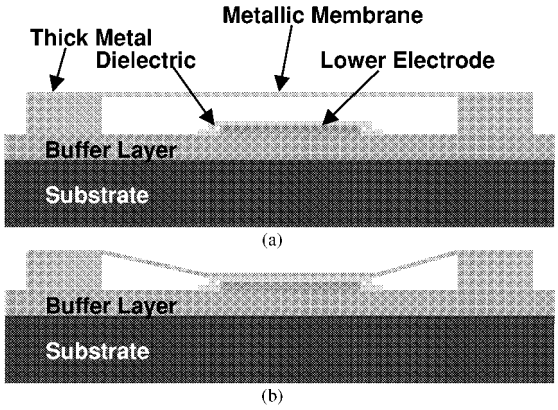

Figure 1. Cross-section of an RF MEMs capacitor in the unactuated (a) and actuated (b) positions.

tric surface, forming a low impedance RF path to ground. Figure 1b demonstrates an RF MEMs capacitive capacitor in the actuated state. In this state, the characteristics of the dielectric layer primarily determine the MEMs on-capacitance. By virtue of changing the position of the membrane with an applied DC voltage, the capacitance of this RF MEMs device can be changed over a significant capacitance range.

The RF MEMs capacitors described in this article are built on high resistivity silicon substrates ($> 10\ \mathrm{k}\Omega$ cm), with a 1 μm thick layer of silicon dioxide used as a buffer layer. The capacitor circuitry is fabricated on top of the silicon dioxide using 4.0 μm thick aluminum interconnects which are compatible with CMOS circuitry and exhibit low conductor losses at high frequencies. The bottom electrode of the capacitors is built using < 0.5 μm of refractory metal. This film provides good conductivity for low loss and has a smooth surface finish. This finish is important for achieving good contact between the membrane and the lower electrode, minimizing any air gap. On top of the lower electrode is a film of silicon nitride, less than 0.3 μm thick. This film blocks the DC control signal from shorting out during capacitor actuation, yet allows RF signals to capacitively couple from the lower electrode to the upper membrane. The metallic capacitor membrane consists of a thin aluminum layer less than 0.5 μm thick. This membrane has high conductivity for low RF resistance and good mechanical properties. The suspended metal membrane spans two grounded posts. A series of 2 μm holes is patterned throughout the upper membrane to accelerate the removal of the sacrificial polymer from beneath the membrane. Removing this material mechanically releases the membrane, freeing it to move up and down onto the lower electrode in response to applied electrostatic forces. A top view of the completed RF MEMs capacitor is shown in Figure 2. The size of the signal path line is 120 μm wide, while the size of the membrane is approximately 120 μm in width and spans 280 μm from ground to ground.

III. MEMs CAPACITOR FABRICATION

Surface micromachining techniques were utilized to fabricate the RF MEMs capacitors described above. Figure 3 demonstrates the essential process steps: 1 A thick insulating thermal oxide is grown on the substrate. 2 A thin layer of refractory metal is deposited and patterned to define the capacitor electrodes. 3 A layer of PECVD silicon nitride is deposited and patterned to form

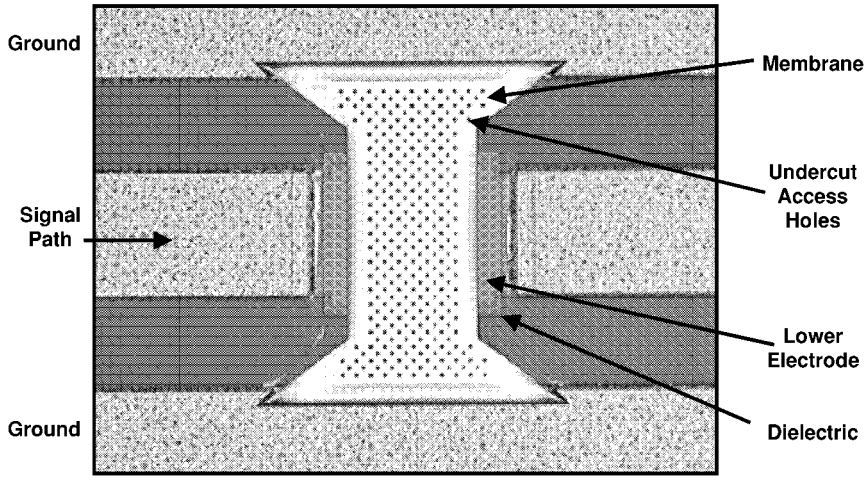

Figure 2. Top view of a shunt MEMs capacitor.

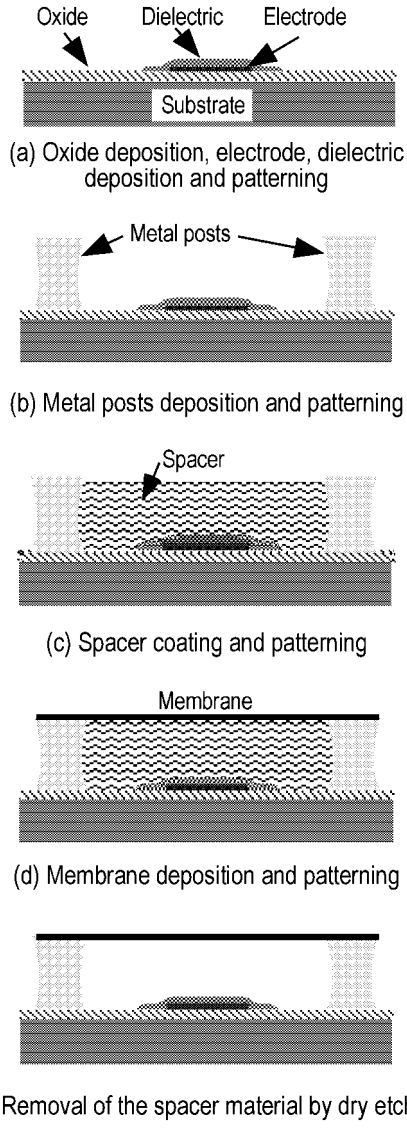

Figure 3. Process flow for fabrication of a MEMs capacitor.

the capacitor dielectric. 4 A thick layer of aluminum is evaporated and patterned to define the metal transmission lines and the mechanical support posts for the capacitor. 5 A polymer sacrificial layer is spin coated and patterned. 6 An aluminum film is deposited and patterned to define the capacitor membrane. 7 The sacrificial layer is removed by a plasma etch through access holes and the edges of the membrane.

IV. MEMs CAPACITOR ELECTRICAL PERFORMANCE

Characterization of the RF MEMs capacitor control element consists of two-port *s*-parameter measurements of a shunt RF MEMs capacitor situated in the middle of a 50 Ω transmission line. Measurements of the *s*-parameters of the capacitor in actuated (on) and unactuated (off) states yields information regarding resistances and reactances at frequencies throughout the microwave spectrum. *s*-parameter measurements were performed over the 0.13–40 GHz frequency range using a Wiltron 37279 vector network analyzer and a Cascade Summit 10000 RF probing system. DC resistance measurements were made with a Fluke 8840A multimeter connected to DC probes. From these measurements, an equivalent circuit model was extracted to determine capacitor element performance.

A physically based electrical model of the RF MEMs capacitor is shown in Figure 4. The two series resistors, R_{SE}, model the contact and path resistance of the capacitor lower electrode. The shunt resistors, R_{SH}, represent the resistive loss from the center of the capacitor element, through the membrane, to ground. As the membrane and electrode are physically thin compared to a skin depth at microwave frequencies, the DC and RF resistances for these physical elements are approximately equal. The capacitance of the membrane in the unactuated state, C_{OFF}, is a function of the area of the membrane and lower electrode, and the height of the air gap. The capacitance of the membrane in the actuated state (C_{ON}) is a function of the area, thickness, dielectric constant, and surface finish of the dielectric layer. As the capacitor element is physically small compared to a wavelength at microwave frequencies, representation of this device as a lumped capacitor is appropriate.

Resistance measurements of the lower electrode yield approximately 0.6 to 1.0 Ω of resistance from end to end. Therefore, R_{SE} is approximately 0.3 to 0.5 Ω. Resistance measurements of

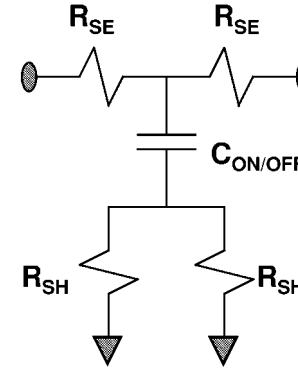

Figure 4. RF model of a MEMs capacitor.

the membrane from end to end yields approximately 0.3 Ω, so R_{SH} is approximately 0.15 Ω. The reactance of the capacitor membrane was determined based on the insertion and isolation performance of the two-port device at microwave frequencies.

Due to the low loss of the RF MEMs capacitors in the off-state, direct measurement of insertion loss tends to be inaccurate. Therefore, comparative loss measurements were made. Figure 5 demonstrates the loss of 1030 μm long CPW transmission lines and RF MEMs capacitors embedded within transmission lines of the same length. Looking at the difference between 1 mm transmission lines with and without MEMs capacitors yields approximately 0.15 dB loss at 10 GHz and 0.28 dB loss at 35 GHz. Variability of the measurements was approximately ± 0.05 dB, mainly due to difficulty in making good contact between the probes and aluminum lines due to the formation of oxides. This value is compatible with the DC resistance of the electrode, with 1 Ω of resistance causing approximately 0.1 dB insertion loss in a 50 Ω system.

The return loss of the RF MEMs capacitor in the off-state is also shown in Figure 5. This reflected energy is due to the parasitic capacitance caused by the proximity of the transmission path to the grounded metal membrane suspended above. The capacitance of the membrane yields approximately 20 dB return loss at 20 GHz. The off-capacitance of the element can be extracted from the formula

$$C_{\mathrm{OFF}} = \frac{\sqrt{-10^{(0.1RL)}/\left(f^2 R_O^2 [10^{(0.1RL)} - 1]\right)}}{\pi}, \tag{1}$$

where RL is the magnitude of measured return loss at frequency f and R_{O} is the system impedance, usually 50 Ω. Typical values of C_{OFF} range from 35 to 50 fF.

When actuated into the on-state, the low suseptance of this capacitor to ground reflects most of the RF energy incident on the element. The two-port isolation caused by this suseptance is shown in Figure 6. This isolation averages 15 dB at 10 GHz and improves to 35 dB at 35 GHz. At frequencies below 30 GHz, the isolation is determined by the effective on-capacitance of the device. Above 30 GHz, the on-capacitance becomes an RF short, and the effective series resistance of the capacitor dominates the isolation. Measurements through 50 GHz do not reveal a monotonic decrease in isolation. This is indicative that the impedance of the membrane capacitor does not go through a series resonance over the frequencies of interest. The effective on-capacitance can be determined from the frequency

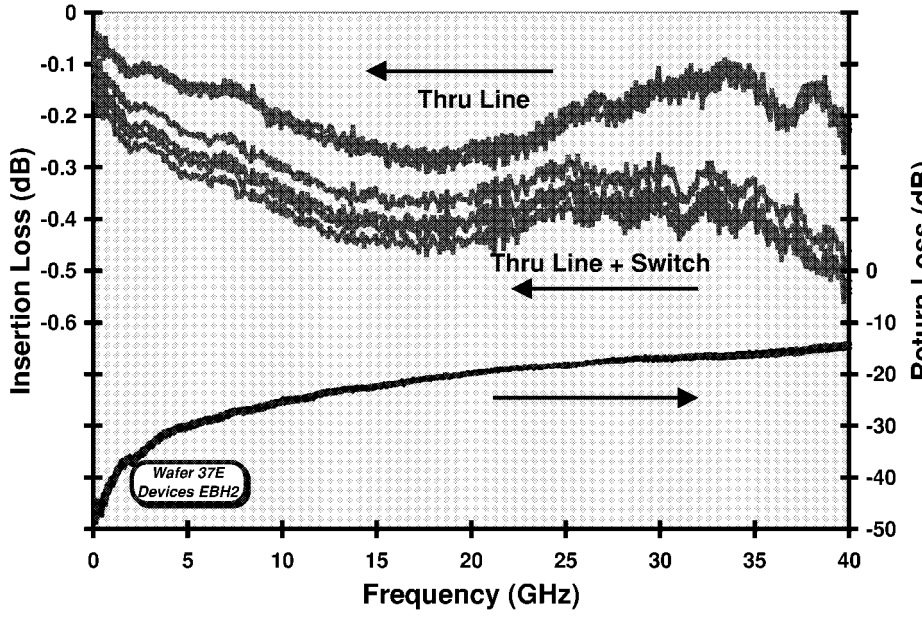

Figure 5. Typical insertion loss and return loss for several (four) unactuated shunt RF MEMs capacitors.

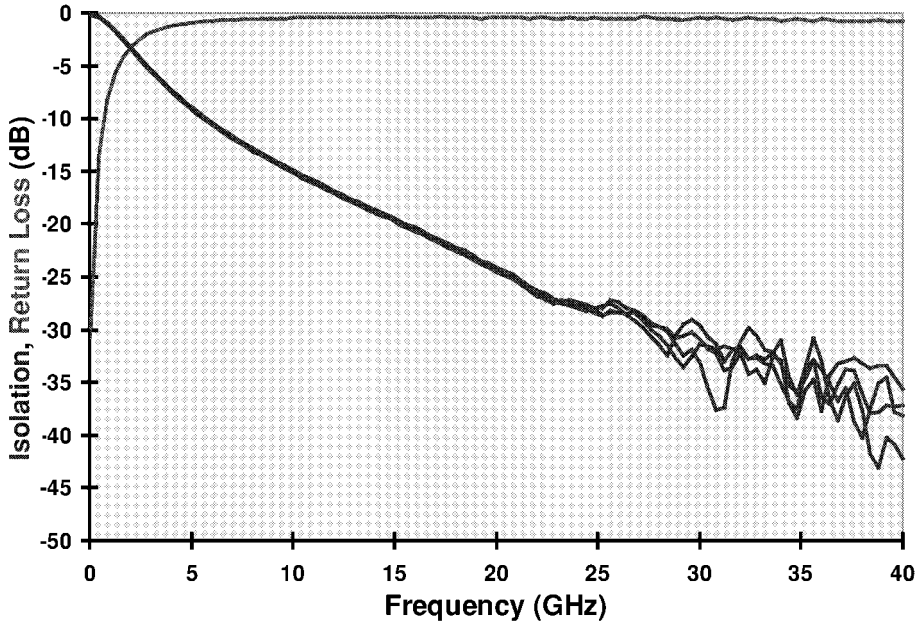

Figure 6. Typical isolation and return loss for several actuated shunt MEMs capacitors.

where the return loss and isolation intersect, at approximately -3 dB. This capacitance is determined from

$$C_{\mathrm{ON}} = \frac{1}{\pi f_C R_O}, \tag{2}$$

where f_C is the -3 dB crossover frequency and R_{O} is the system impedance. Inspection of the graph shows this crossover frequency to be slightly less than 2 GHz. Data of this type reveals that typical membrane on-capacitance ranges from 3.2 to 3.6 pF. The ratio of on-state to off-state capacitance for these devices generally runs between 70:1 and 100:1. Such a high on/off ratio allows for fabrication of variable MEMs capacitors with an overall large capacitance change, as will be presented later in this paper.

V. MEMs CAPACITOR MECHANICAL PERFORMANCE

The actuation voltage for these capacitors is determined primarily by the spring constant of the mechanical system of the membrane. The applied voltage, membrane geometry, membrane material properties, and gap height between the membrane and the bottom electrode determine the mechanical position of the membrane. A first-order solution of the pulldown voltage can be calculated by analyzing the following pressure balance equation [5]:

$$P_e(g) = K_s(g_o - g) - \frac{\epsilon V^2}{2g^2}, \tag{3}$$

where P_e is the uniform electrical pressure on the membrane, K_s is the spring constant of the mechanical system, g is the height of the capacitor body above the bottom electrode, g_o is the initial height of g with no applied load, V is the applied electrostatic potential, and ϵ is the permittivity. It is derived based on a lumped model consists of a single parallel-plate capacitor suspended above a ground plane by an ideal linear spring. The model has a single degree of freedom, the gap between the movable plate and the fixed ground plate. The pulldown voltage for this system can be solved as

$$V_p = \sqrt{\frac{8K_s g_o^3}{27\epsilon}}. \tag{4}$$

To use the above equation, one only needs to know the spring constant for the problem at hand. For a clamped/clamped beam, the spring con-

stant can be obtained by analyzing the associated governing differential equation

$$\tilde{E}I\frac{d^4g}{dx^4} + \sigma(1-\nu)wt\frac{d^2g}{dx^2} = -\frac{\epsilon V^2 w}{2g^2} + Pw. \tag{5}$$

The result [5] is

$$K_s = \frac{32\tilde{E}t^3}{L^4} + \frac{8\sigma(1-\nu)t}{L^2}, \tag{6}$$

where $\tilde{E}$ is the effective modulus, t is the beam thickness, L is the beam length, w is the beam width, σ is the biaxial residual stress, ν is the Poisson's ratio, P is the pressure, and I is the moment of inertia with respect to the long axis of the beam. For narrow beams $\tilde{E}$ is the Young's modulus E, while for wide beams

$$\tilde{E} = \frac{E}{1-\nu^2}. \tag{7}$$

The pulldown voltage predicated by eq. (4) could be significantly in error because the deformable capacitor is represented by a rigid plate. Both the position dependent electrostatic load and a first-order fringing field correction term were considered in an improved 2D distributed model. The governing equation is

$$\tilde{E}I\frac{d^4g}{dx^4} + \sigma(1-\nu)wt\frac{d^2g}{dx^2} = -\frac{\epsilon V^2 w}{2g^2}\left(1 + 0.65\frac{g}{w}\right). \tag{8}$$

The equation is nonlinear and was solved numerically [6]. The closed-form expression for pulldown voltage is

$$V_P = \sqrt{\frac{2.79[\sigma(1-\nu)]}{\epsilon L^2 D[1 + 0.42(g_o/w)]}}, \tag{9}$$

where

$$D = 1 + \frac{2[1-\cosh(A)]}{A\sinh(A)}$$

and

$$A = 0.485L\sqrt{\frac{12\sigma}{\tilde{E}t^3 g_o^3}}. \tag{10}$$

Though eq. (10) can be used directly for prediction of pulldown voltage it assumes that the bottom electrode has an area no less than the top membrane and has the following limitations [7]:

(1) Structures must be nearly parallel.
(2) Structures must have a small gap to length aspect ratio.
(3) Structures must have a good fixed boundary condition.
(4) Gap must be small compared to the membrane thickness.

For the RF MEMs capacitors described in this article, not only is the gap (> 3 μm) much larger than the membrane thickness (< 0.5 μm), but also the effective area of the bottom electrode is much less than that of the membrane. In addition, the movable electrode is not a rectangular membrane and has a series of 2 μm holes patterned throughout it. These complexities necessitate that an accurate pulldown voltage be computed by use of a full 3D numerical simulation.

The commercial simulation package IntelliCAD [8] was used to compute the membrane pulldown voltages. With residual stresses in the 20–100 MPa range, the actuation voltages range from 24 to 56 Vs. The pulldown voltages obtained by using eqs. (4), (9), and IntelliCAD are shown in Figure 7. The results of eq. (9) are 6% to 8% higher than that of eq. (4). The results of IntelliCAD are 12% to 17% higher than which of eq. (9). In both cases, a higher residual stress gives a larger difference. The residual stress is initially dependent on the deposition conditions of the membrane on the top of sacrificial layer, but is later modified by the fabrication of access holes in the membrane, as well as the release of the membrane from the sacrificial layer. The measured typical actuation voltages range from 30 to 55 V.

A nonlinear dynamic model that captures the effects of electrostatics, deformation, residual stress, inertia, damping, Van der Waals force, impact, contact, and air dynamic is essential for

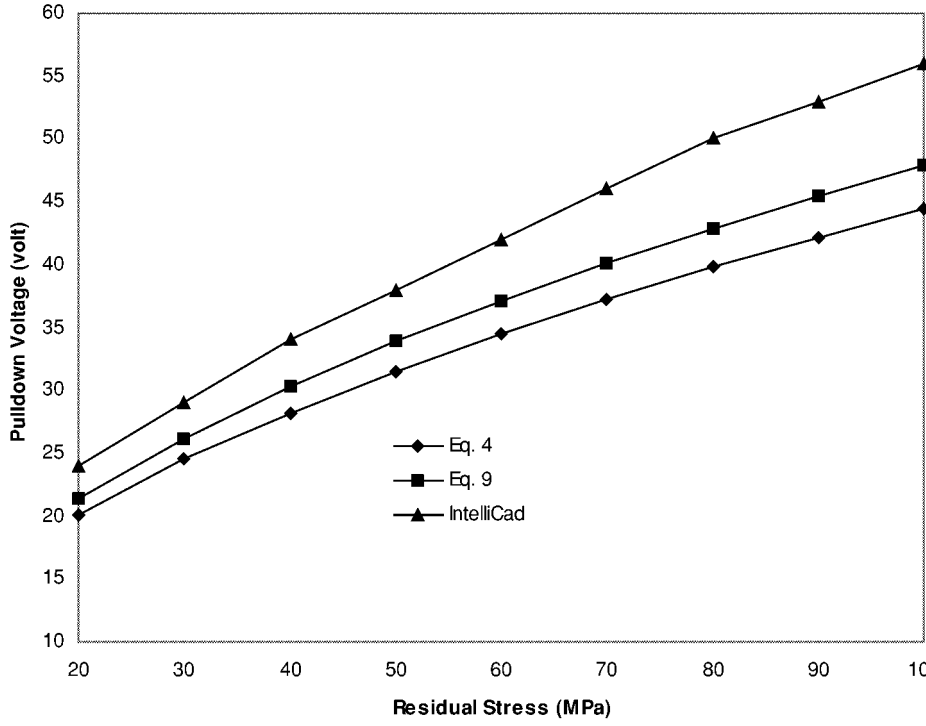

Figure 7. Pulldown voltages vs. membrane residual stresses.

an accurate switching speed evaluation. There is neither a closed form solution nor simulation tool for MEMs dynamics at present. As a first-order approximation, the switching speed of these devices can be determined by the mechanical primary natural frequency of the devices. The membrane moves from the contact position to its mechanically neutral position when there is no electrostatic force exerted on it. By neglecting damping, Van der Waals force, impact, contact, and air dynamic effects, this release time can be approximated by 1/4 period of the membrane free vibration because there is no external force exerted on the membrane. The membrane actuation time will be even quicker, due to the applied electrostatic force. Finite element analyses using ABAQUS [9] show that the primary frequencies of these devices ranged from 56 to 150 kHz depending on the magnitude of residual stresses. This puts the theoretical switching speed in the 1.67–4.5 μs range. Typical measured switching turn-on and turn-off times range from 3 to 6 μs. The high mechanical resonant frequencies and fast switching speeds of these devices allows for quick tuning of capacitor elements. This makes for high speed tuning of oscillators and receiver front-ends, necessary for many modern communications modulation schemes.

The turn-on and turn-off switching waveforms for the MEMs capacitor is shown in Figure 8. It should be noted that these waveforms were taken without any dielectric charging present. When actuating MEMs capacitors on and off, it is possible for the high electric field across the thin dielectric to cause charges to tunnel into the dielectric and become trapped. These charges screen the applied electric field, causing the MEMs capacitor to need higher switching voltages and causing some problems with using unipolar DC control voltages. Techniques to mitigate this charging are an area of on-going research.

VI. VARIABLE CAPACITOR CONSTRUCTION

A voltage controlled variable capacitor (varactor) can be constructed using switchable MEMs capacitors as the control element. As the MEMs capacitors are binary (on/off) controlled, the most

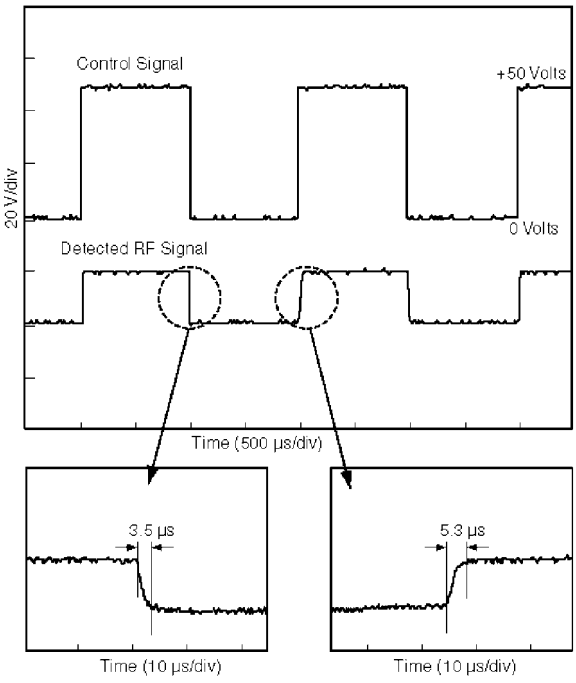

Figure 8. Typical switching speed measurements for a MEMs capacitor.

useful configuration for a variable capacitor is with binary weighted capacitance selection. The schematic of one possible topology is shown in Figure 9. This arrangement constructs each binary capacitor bit as a single branch containing one or more MEMs capacitors and a fixed capacitor. The total capacitance of each branch is the series combination of the two sets of capacitors. In the schematic, the largest bit consists of six switchable MEMs capacitors at 3.4 pF each for a total of 20 pF in combination with the series 74 pF capacitor. This yields the desired 16 pF of total capacitance for the largest bit. The smaller bits are similarly constructed, and contain 8, 4, 2, 1, and .5 pF total capacitance. The bits with a total capacitance of less than 3.4 pF use a single capacitor membrane, and a series capacitor that acts as a divider to reduce the total capacitance to the desired value. For example, the smallest bit is realized with a single MEMs capacitor in series with a 0.6 pF capacitor, with an effective capacitance of 0.5 pF when the MEMs capacitor is actuated.

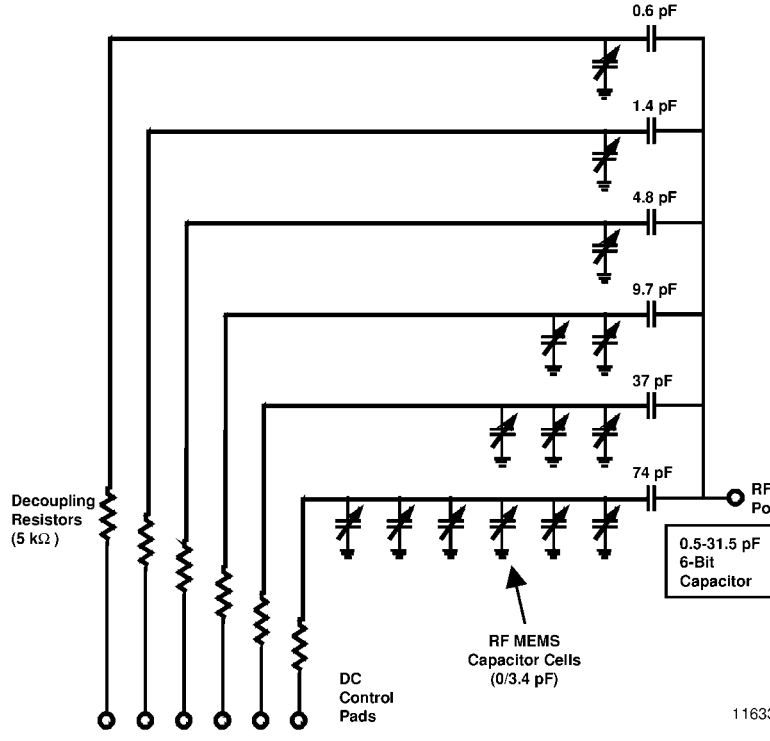

Figure 9. Schematic of a tunable capacitor using numerous shunt MEMs capacitor elements.

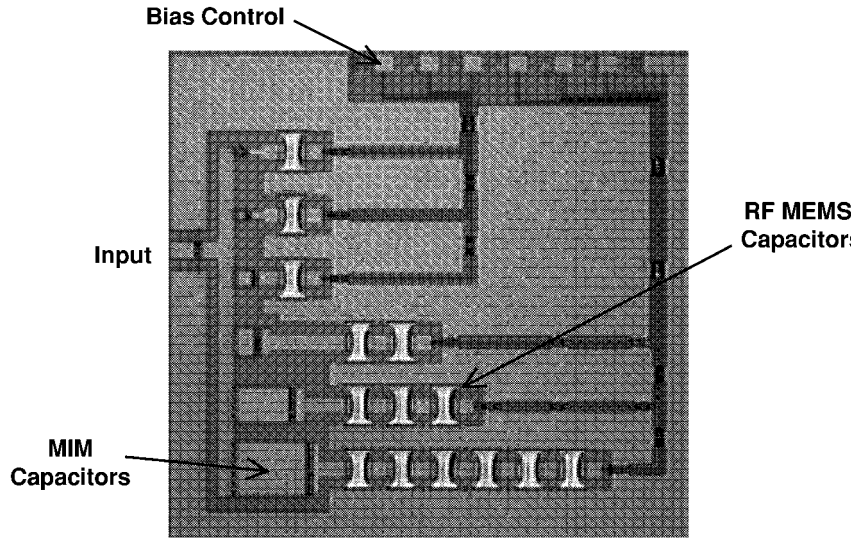

Figure 10. Micrograph of a tunable RF MEMs capacitor.

Each of the MEMs capacitors is actuated by application of a control voltage to the capacitor electrode. Each control signal is decoupled from the RF through a 5 kΩ thin-film resistor. The series capacitor serves to block the control voltage from interfering with adjoining circuitry. As each MEMs draws negligible current, biasing the device through a high resistance serves as an effective means of minimizing DC–RF interactions.

A completed RF MEMs shunt variable capacitor is shown in Figure 10. The overall chip size is 3.2×3.2 mm $\times$ 0.53 mm. The layout of the device was not optimized for minimum size, and was laid out in a fashion very similar to the schematic. The capacitor RF port is on the left side of the chip while the DC control pads are on the top of the IC. Unused areas were filled with ground plane to minimize coupling between bits and the DC control lines.

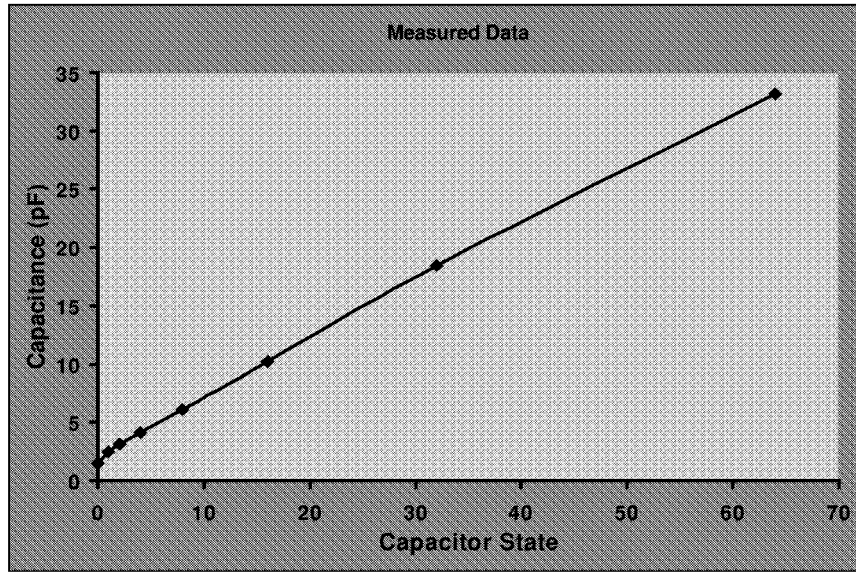

Figure 11. Capacitance of the tunable MEMs capacitor vs. binary state.

The measured capacitance of the variable capacitor ranges from 1.5 pF with none of the bits actuated to 33.2 pF with all of the bits actuated. A graph of this response is shown in Figure 11. This represents a maximum on/off ratio of approximately 22; the highest the authors believe has been reported to date. The highest five bits of the capacitor exhibit a differential capacitance within 5% of the desired values. The smallest bits are impacted by fringing capacitance of the interconnects. The off-capacitance of the 14 individual MEMs capacitors is approximately 500–700 fF. Therefore, a bulk of the 1.5 pF zero-state capacitance is due to fringing between the capacitor interconnects and the closely spaced ground plane. With proper layout to reduce this parasitic capacitance, capacitance tuning ranges in the 40–50 range should be achievable. Figure 12 demonstrates the capacitance of the IC as a function of frequency. As the IC is actuated through its various states, the variable capacitor changes series-resonant frequency. This change is a function of the capacitance to ground in each state, and the line length between the input and that capacitance. Future designs will be improved by reducing all line lengths, and by positioning the larger capacitance states (which are more sensitive to line length) closer to the input terminal. The quality factor (Q) of this variable capacitor is less than 20 at 1 GHz. This is due mainly to the long line lengths and the addition of the multiple electrode resistances in series. Future designs will modify the connections between membranes to a more parallel arrangement, greatly reducing the overall resistance. It is estimated that quality factors greater than 50 are achievable with improved layout and thicker conductor interconnects.

VII. TUNABLE FILTER TOPOLOGY

One challenge in designing tunable filters with variable capacitors is finding a means to tune the center frequency without having to tune inductors. Typically, filters are tuned by changing both inductors and capacitors. As an example, the schematic of a third-order bandpass filter designed using modern synthesis techniques is shown in Figure 13a. The prototype element values are designed to yield a desired passband filter response. This filter can be scaled to any desired impedance and frequency by the appropriate scaling techniques. Changing the center frequency of the filter while maintaining a given bandwidth requires tuning the shunt capacitors and series inductors within each of the series and shunt resonators of the filter. Unfortunately, this means that tuning the filter requires more than just

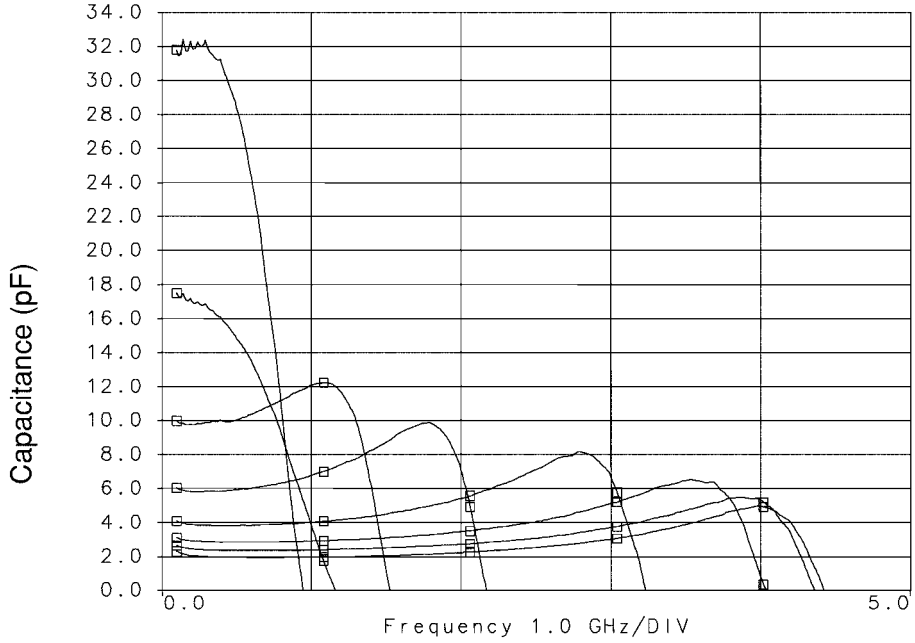

Figure 12. Capacitance of a tunable MEMs capacitor vs. frequency.

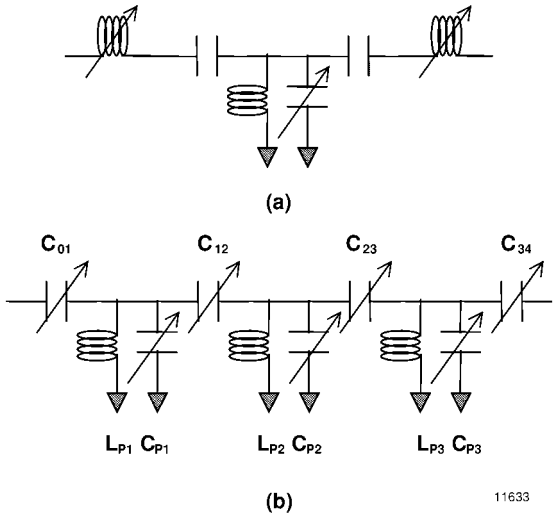

Figure 13. Conventional bandpass filter topology (a) and one utilizing impedance inverters (b).

tunable capacitors, but variable inductors as well. A tunable filter with fixed inductors and tunable capacitors is desirable for implementations using only tunable capacitors such as those described above.

One common technique for constructing microwave bandpass filters involves using impedance inverters to convert series resonators to shunt, parallel resonators. By use of inverters, a filter with both series and shunt resonators can be converted to a filter that has only shunt resonators. An example of this filter topology is shown in Figure 13b. An added benefit of this design is that redundant elements add an extra degree of freedom to the design. This extra degree allows all inductors to remain fixed and constant as the filter center frequency is tuned. This is a key ingredient to designing filters that are electronically tuned by varying RF MEMs capacitors.

Detailed design procedures for the design of lumped element filters incorporating impedance inverters can be found in several texts [10]. The design process is summarized as follows. In designing a filter of order N, the normalized element values for the filter, g_0 through g_N, must be determined [11]. The fractional bandwidth, a, is set by

$$a = \frac{\omega_O}{\omega_H - \omega_L}, \tag{11}$$

where ω_O is the desired center frequency and ω_H and ω_L are the desired upper and lower cutoff frequencies, respectively. Next, a normalized value for the shunt inductors, L_i, is picked. This value is arbitrary and can later be scaled to achieve the desired inductor and capacitor values. To resonate at a normalized frequency of 1 rad/s, the values for C_i are simply

$$C_i = \frac{1}{L_i}. \tag{12}$$

Next, the impedance inverter values are designed based on the normalized element values, g_i, and the capacitor value C_i, with

$$J_{01}^2 = \frac{C_1 a}{g_0 g_1}, \qquad J_{i,i+1}^2 = \frac{a^2 C_i C_{i+1}}{g_n g_{n+1}}$$
$$J_{N,N+1}^2 = \frac{C_N a}{g_N g_{N+1}}. \tag{13}$$

Next, the series caps that comprise the center portion of the impedance inverters are designed as

$$C_{01} = \sqrt{\frac{1}{(1/J_{01}^2 - 1)}}, \qquad C_{i,i+1} = J_{i,i+1},$$
$$C_{N,N+1} = \sqrt{\frac{1}{\left[(1/J_{N,N+1}^2) - 1\right]}}. \tag{14}$$

The shunt capacitor element values are now finally determined by the normalized capacitor values, C_i, and the impedance inverters as

$$C_{P1} = C_1 - \frac{C_{01}}{1 + C_{01}^2} - C_{12},$$
$$C_{Pi} = C_i - C_{i-1,i} - C_{i,i+1},$$
$$C_{PN} = C_N - C_{N-1,N} - \frac{C_{N,N+1}}{1 + C_{N,N+1}^2}. \tag{15}$$

The shunt inductor values are simply $L_{Pi} = L_i$. This completes the design for a filter impedance normalized to 1 Ω and frequency normalized to 1 rad/s.

Using the equations above, normalized bandpass filters were scaled to 50 Ω and designed for 1, 1.5, and 2 GHz center frequencies. In all cases, the bandwidth was maintained at 200 MHz. The

TABLE 1. Tuned filter element values.

	1000 MHz	1500 MHz	2000 MHz
C01	5.850	1.533	0.778 pF
Cp1	9.002	3.932	2.247 pF
Lp1	2.000	2.000	2.000 nH
C12	2.329	0.690	0.291 pF
Cp2	8.009	4.249	2.584 pF
Lp2	2.000	2.000	2.000 nH
C23	2.329	0.690	0.291 pF
Cp3	9.002	3.932	2.247 pF
Lp3	2.000	2.000	2.000 nH
C34	5.850	1.533	0.778 pF

resulting element values are shown in Table 1. By varying the value of L_i to compensate for the frequency tuning, the inductor values can be kept constant. This is key to designing filters with capacitor-only tuning. However, keeping the inductors constant as the frequency is tuned requires retuning the impedance inverters as well as the resonators. This means that some capacitors may tune much more than they would with conventional filters, where the capacitors and inductors tune inversely proportional to the square of the frequency change. Inspection of this table shows that the capacitors tune by varying amounts, ranging from a 3:1 to 8:1 ratio for a 2:1 frequency change. Therefore, this method of designing tunable filters requires significant capacitor tuning ranges. This reinforces the motivation for using a capacitive membrane tuning technique such as presented in this paper, which allows for a wide tuning range.

VIII. CONCLUSION

A MEMs capacitive tuning technique has been presented which exhibits a large tuning range and relatively quick switching times. Through the use of surface micromachining techniques, MEMs capacitor elements have been fabricated which operate through 40 GHz with a tuning ratio in the range of 70:1 to 100:1, control voltages in the 30–50 V range, and switching times less than 10 μS. These devices have been utilized to fabricate a six-bit variable capacitor with a tuning range from 1.5 to 33.2 pF of capacitance. This represents a significant improvement over previous RF MEMs variable capacitors. A design technique has been introduced which allows these devices to be eventually used to make high performance tunable filters using only capacitor tuning. These tunable filters will have application in a variety of tunable filter, oscillator, and receiver applications.

ACKNOWLEDGMENTS

This research and development was sponsored by DARPA under Contract No. F30602-97-C-0186. The authors would like to thank Tommy Smith for process support and Chip Perry and Dallas White for layout support.

REFERENCES

1. D. Young and B. Boser, A micromachined variable capacitor for monolithic low-noise VCOs, IEEE Solid State Sensor Conf (1996), 86–89.
2. E.S. Hung and S.D. Senturia, Tunable capacitors with programmable capacitance-voltage characteristic, IEEE Solid State Sensor Conf (1998), 292–295.
3. A. Dec and K. Suyama, RF micromachined varactors with wide tuning range, IEEE Microwave Theory Tech Symp (1998), 357–360.
4. H.D. Wu, K.F. Harsh, R.S. Irwin, W. Zhang, A.R. Mickelson, and Y.C. Lee, MEMs designed for tunable capacitors, IEEE Microwave Theory Tech Symp (1998), 127–129.
5. P. Osterberg, H. Yie, X. Cai, J. White, and S. Senturia, Self-consistent simulation and modeling of electrostatically deformed diaphragms, Proc MEMs 94 Osio, Japan, Jan. 1994, 28–32.
6. P.M. Osterberg, R.K. Gupta, J.R. Gilbert, and S.D. Senturia, Quantitative models for the measurement of residual stress, poisson's ratio and Young's modulus using electrostatic pull-in of beams and diaphragms, Solid-state sensor and actuator workshop, Hilton Head, South Carolina, June 13–16, 1994, 184–188.
7. P.M. Osterberg, Electrostatically actuated microelectromechanical test structures for material property measurement, Ph.D thesis at MIT, 1995.
8. IntelliCAD Version 3.5, IntelliSense Corporation, 16 Upton Drive, Wilmington, MA 01887.
9. ABAQUS/Standard Version 5.7, Hibbitt, Karlsson & Sorensen, Inc. 1080 Main Street, Pawtucket, RI 02860-4847.
10. White Electromagnetics, A Handbook on Electrical Filters, White Electromagnetics, Rockville, MD, 1963.
11. A.I. Zverev, Handbook of Filter Synthesis, John Wiley & Sons, 1967.

BIOGRAPHIES

Charles L. Goldsmith For bio and photo see p. 309.

Andrew Malczewski was born in Warsaw, Poland in May, 1973. He earned a Bachelor's degree in Electrical Engineering from the University of Texas at Arlington in 1996. Since 1996, he has been involved in the design and development of microwave-wave circuits for Raytheon Systems Company (formerly the Defense Electronics Group of Texas Instruments). He is also involved in the development of RF MEMs technology for receiver and antenna applications. He is presently pursuing his Master's degree in Electrical Engineering.

Zhimin J. Yao received her Ph.D. from the School of Materials Science and Engineering at Georgia Institute of Technology in 1995. She then worked as a post doctoral research associate at the School of Electrical Engineering, Cornell University for one year. Her research emphasis was on silicon bulk micromachining. Dr. Yao is currently working at Applied Research Laboratories of Raytheon Systems Company (formerly the Center of Research and Development of Texas Instruments). Her research interest include design, fabrication and characterization of microelectromechanical systems.

Shea Chen was born in Taichung, Taiwan, Dec. 1951. He received his Bachelor's degree in Mechanical Engineering from Tamkang University in Taiwan in 1976. He received his Master's degree in Mechanical Engineering from the University of Texas at Arlington in 1980. In 1991 he earned a Ph.D. in Mechanical Engineering from Southern Methodist University. He has been an RF/Microwave mechanical engineer at Raytheon Systems Company (formerly the Defense Electronic Group of Texas Instruments) since 1995 and involved in the structural analysis, the POF evaluation, the fatique life estimation and the integrity prediction for microelectronic devices and microwave components, and the mechanical design/analysis for microelectromechanical switches. Dr. Chen is an associate member of ASME.

John Ehmke was born in Knoxville, Iowa. He earned a Bachelor's in Physics from Bob Jones University in 1983. In 1985 he earned his Master's in Physics from Purdue University. He has worked at Raytheon Systems Company, formerly Texas Instruments Defense Systems and Equipment Group, since 1985. Most of that time has been applied to the development of 2nd generation IR focal plane arrays. He has been working since 1997 on RE MEMs devices for antenna and receiver applications. Mr. Ehmke has authored several patents and is a member of the IEEE.

David H. Hinzel received BS degrees in Physics and Mathematics from Kent State University, a BSEE from the University of Massachusetts at Amherst, an MSEE from the George Washington University in Washington, D.C., and has completed coursework for the DScEE degree at the George Washington University. He has worked for General Electric, the BDM Corporation, Litton Amecom, E-Systems, and Raytheon Systems Company. In addition, he is the co-founder of Eagle Eye Technologies, Inc., a small startup business developing satellite based tracking services. At Raytheon Systems Company, he is currently the RF technical lead for an advanced digital receiver/transmitter program and is developing RF MEMs turnable filters in support of that effort.